Draft version February 5, 2024
Typeset using LaTeX **twocolumn** style in AASTeX62

# A New Catalog of 100,000 Variable *TESS* A-F Stars Reveals a Correlation Between $\delta$ Scuti Pulsator Fraction and Stellar Rotation

Keyan Gootkin,[1] Marc Hon,[1,2] Daniel Huber,[1,3] Daniel R. Hey,[1] Timothy R. Bedding,[3] and Simon J. Murphy[4]

[1] *Institute for Astronomy, University of Hawai'i, 2680 Woodlawn Drive, Honolulu, HI 96822, USA*
[2] *Kavli Institute for Astrophysics and Space Research, Massachusetts Institute of Technology, 77 Massachusetts Avenue, Cambridge, MA 02139, USA*
[3] *Sydney Institute for Astronomy, School of Physics, University of Sydney NSW 2006, Australia*
[4] *Centre for Astrophysics, University of Southern Queensland, Toowoomba, QLD 4350, Australia*

## ABSTRACT

$\delta$ Scuti variables reside at the intersection of the classical instability strip and the main sequence on the Hertzsprung-Russell diagram. Despite our understanding of the underlying mechanisms driving pulsations in $\delta$ Scuti stars, many stars within the instability strip do not pulsate. With space-based photometry providing millions of light-curves of A-F type stars, we can now probe the occurrence rate of $\delta$ Scuti pulsations in detail. Using 30-min cadence light-curves from NASA's Transiting Exoplanet Survey Satellite's (TESS) first 26 sectors, we identify variability in 103,810 stars within 5-24 cycles per day down to a magnitude of $T = 11.25$. We fit the period-luminosity relation of the fundamental radial mode for $\delta$ Scuti stars in the *Gaia* $G$-band, allowing us to distinguish classical pulsators from contaminants for a subset of 39,367 stars. Out of this subset, over 15,920 sit on or above the expected period-luminosity relation. We derive an empirical instability strip using *Gaia* photometry and find that pulsator fraction peaks at 50-70%. While many variable sources sit below the period-luminosity relation, over 85% of sources inside of the classical instability strip derived in this work are consistent with being $\delta$ Scuti stars. The remaining 15% of variables within the instability strip are likely hybrid or $\gamma$ Doradus pulsators. Finally, we discover strong evidence for a correlation between pulsator fraction and spectral line broadening from the Radial Velocity Spectrometer (RVS) aboard the *Gaia* spacecraft, confirming that rotation has a role in driving pulsations in $\delta$ Scuti stars.

## 1. INTRODUCTION

$\delta$ Scuti variables are stars of spectral type A0-F5 on or near the main sequence and within the classical instability strip, with luminosities of roughly $2 - 50 L_\odot$ and masses of roughly $1.5{-}2.3 M_\odot$ (Breger 1979; Goupil et al. 2005; Handler 2009a; Guzik 2021; Kurtz 2022). Similar to Cepheids, these stars follow a period-luminosity relation which allows them to be used as "standard candles" within the Milky Way and Magellanic Clouds (i.e. Leavitt 1908; McNamara et al. 2007; Majaess et al. 2011a,b).

In theory, any star inside of the instability strip should have the partial ionization layers which drive $\delta$ Scuti pulsations through the $\kappa$-mechanism (Dupret, M.-A. et al. 2004, 2005). Murphy et al. (2019) used *Kepler* data to detect pulsations in 1988 stars and showed that the fraction of stars which are pulsators peaks at only 70% in the center of the instability strip using a sample of over 15,000 A-F stars in the Kepler field. While the distribution of observed pulsation frequencies in many $\delta$ Scuti stars have been reported to correlate with the stars' fundamental properties (Balona & Dziembowski 2011; Barceló Forteza, S. et al. 2018; Bowman & Kurtz 2018; Hasanzadeh et al. 2021), such findings have not been universal (Murphy et al. 2019; Balona 2024; Bedding et al. 2023).

Because of the $\kappa$-mechanism's reliance on the presence of helium at a particular depth within a star, this mechanism must be affected by the chemical structure of a star (Guzik et al. 2018). Chemically peculiar stars such as the metallically lined A-stars (Am stars) have very low pulsator fractions (Breger 1970; Kurtz 1989; Guzik et al. 2021). Am stars are notably slow rotators, which is thought to suppress the $\kappa$-mechanism via gravitational settling of helium out of the ionization zone which drives pulsation (Pamjatnykh 1974; Dziembowski 1980; Ouazzani et al. 2015). This diffusion processes has been invoked to explain observations that $\delta$ Scuti stars tend to be moderate or rapid rotators (Solano &

Corresponding author: Keyan Gootkin
gootkin@hawaii.edu

Fernley 1997; Molenda-Zakowicz et al. 2009). However, these studies were limited by small sample sizes of 10s to 100s of stars.

A challenge with using Kepler data to investigate the occurrence rate of $\delta$ Scuti stars is its complex selection function, which focused on solar-type stars to detected transiting exoplanets (Batalha et al. 2010; Wolniewicz et al. 2021). A larger sample of $\delta$ Scuti variables that is only limited in magnitude will be valuable to verify the instability strip and to examine trends in pulsation properties (i.e. frequency and amplitude) with other stellar quantities. This paper will expand upon the work done in the Kepler field by using NASA's Transiting Exoplanet Survey Satellite (*TESS*; Ricker et al. 2015). Over 4 years *TESS* has provided photometry of tens of millions of stars spread across the sky. Because *TESS* surveys the entire sky without a particular selection function, it allows the most expansive investigation of $\delta$ Scuti pulsators conducted to date (Antoci et al. 2019; Balona & Ozuyar 2020; Barac et al. 2022; Skarka, M. et al. 2022; Xue et al. 2023; Read et al. 2024).

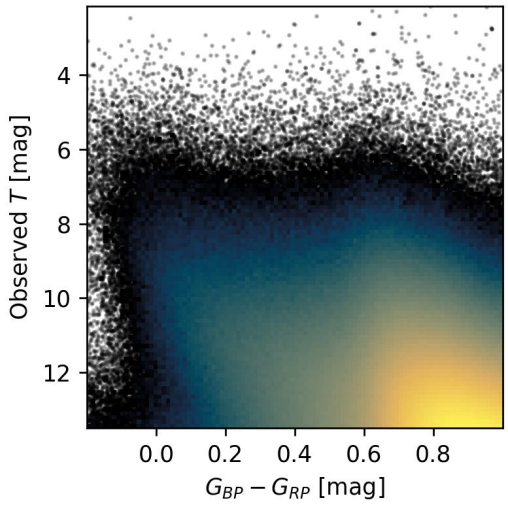


**Figure 1.** A 2D histogram showing the density of all 6,884,170 targets in our sample shown in color versus apparent *TESS*-magnitude. For bins (where each bin is 0.012 mag × 0.115 mag in size) without at least 10 objects we plot the positions of stars as a scatter plot. These quantities have not been corrected for reddening or extinction.

## 2. OBSERVATIONS & TARGET SELECTION

### 2.1. *Sample Selection*

We initially construct our sample from the *TESS* Input Catalog (TIC) based on the *Gaia* color, $G_{BP} - G_{RP}$. We choose bounds which surround the classical instability strip near to the main-sequence ($-0.2 < G_{BP} - G_{RP} < 1$) according to synthetic photometry from MIST models of main-sequence, solar metallicity stars (MESA (Modules for Experiments in Stellar Astrophysics) Isochrones & Stellar Tracks; Paxton et al. 2010, 2013, 2015; Dotter 2016; Choi et al. 2016). There are 6,884,170 objects which fit the constraints $-0.2 < G_{BP} - G_{RP} < 1$ and $T < 13.5$ (the *Full Sample* as described in §3.4). The distribution of this sample in color and apparent *TESS* magnitude is shown in Figure 1.

### 2.2. TESS *Light-Curves*

We use Quick-Look Pipeline light-curves (QLP; Huang et al. 2020a,b; Kunimoto et al. 2021), which were generated from *TESS*'s 30-minute cadence Full-Frame Images (FFIs), for sectors 1-26. The QLP has published light-curves for every observed target in the *TESS* FFIs with $T < 13.5$. From each light-curve we extracted the time, KSPSAP flux which has slow trends and systematics removed, flux error, and quality columns. We selected only timestamps with a quality flag of 0, the strictest quality standard available. From the *Full Sample* we have analyzed such light-curves for 754,909 sources, we refer to these sources as our *Processed Sample* (§3.4).

Each sector was analyzed separately, and not combined with other sectors for the same star. We do this to ensure a uniform treatment of data, irrespective of location on the sky and therefore number of sectors observed. Where multiple sectors of data are available, we use data from the sector with the most statistically significant result (as described in §3).

### 2.3. *Interstellar Extinction*

We correct for extinction using the 3D dust map from Leike et al. (2020), via the Python package `dustmaps` (Green 2018). For each of the targets we integrate the extinction density along the line of sight towards the target. For the reddening—$E(G_{BP} - G_{RP})$—we estimate the extinction in $G_{BP}$ and $G_{RP}$ by fitting the extinction law from Fitzpatrick (1999) to the extinction in $G$. Using this method we can correct the color-magnitude diagram (CMD) locations for 56.9% of the stars which had at least one sector of *TESS* data, or nearly 430,000 targets (the *Dust Corrected* sample as described in §3.4). Since the Leike et al. (2020) dust map is defined in a 740 pc × 740 pc × 540 pc box centered on the Sun, this method biases our *Dust Corrected* sample towards the nearest A-F type stars, but maintains full-sky coverage.

## 3. METHODOLOGY

### 3.1. *Amplitude Spectrum Calculation*

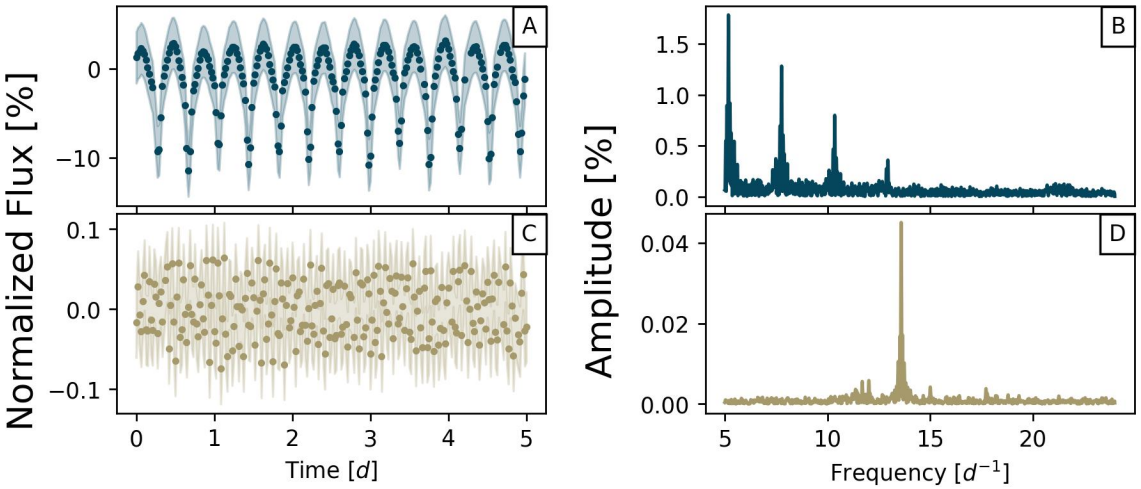


**Figure 2.** Light-curves (panels A and C) and amplitude spectra (panels B and D) of the known eclipsing binary TIC 14842303 in sector 14 (TYC 2697-130-1; panels A and B; Kirk et al. 2016) and the $\delta$ Scuti variable star TIC 67991192 ($\gamma$ Boo; panels C and D) in sector 16. These are representative examples of their respective categories, and illustrate the differences which allow for the identification of pulsators as described in §3.3.

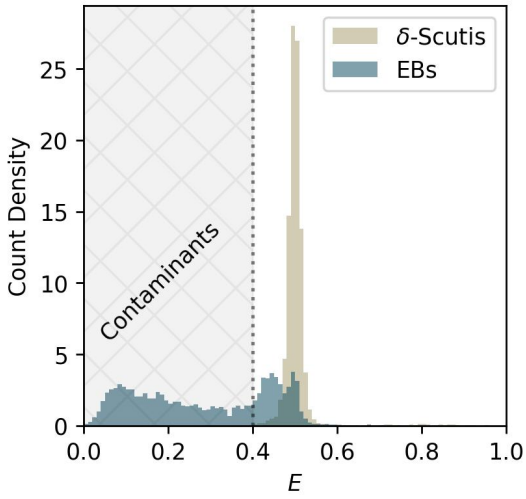


**Figure 3.** Histograms of $E$-parameters for Murphy et al. (2019)'s sample of $\delta$ Scuti variables in gold and a sample of eclipsing binaries from Kirk et al. (2016) in dark blue. The grey hatched region shows the range of values which would result in marking an object an *Eclipsing Binary* in table 1.

For each of the light-curves—created from each sector of observations of each star—we calculate a Lomb-Scargle periodogram (Lomb 1976; Scargle 1982; VanderPlas 2018) using `AstroPy`'s `LombScargle` method (Robitaille et al. 2013; Price-Whelan et al. 2018). We analyze each sector of data for each source seperately. The periodograms presented in this work were calculated between 5 and 24 cycles per day ($d^{-1}$). The lower limit of 5 $d^{-1}$ is a standard cut-off to exclude low frequency pulsations that are characteristic of other types of pulsators, such as $\gamma$ Doradus variables (Handler & Shobbrook 2002; Hareter et al. 2010). It is worth noting, however, that this might remove the highest-luminosity $\delta$ Scuti stars, which can have frequencies below this cut-off (see Fig. 2 in Barac et al. 2022). The upper limit—24 $d^{-1}$—is the Nyquist frequency for 30-minute cadence *TESS* FFI observations. This upper limit will significantly limit the ability to detect the highest frequency $\delta$ Scuti pulsators (e.g. Figure 9 of Hey et al. 2021), which will only be detected by attenuated aliases of the true pulsation frequency mirrored across the Nyquist frequency (Bedding et al. 2020).

### 3.2. *Variability Identification*

We use the method described in Baluev (2008) to estimate the false alarm probability (FAP) for peaks in our amplitude spectra. FAP is the probability that white noise could produce a single peak of a given amplitude. For the purposes of this paper we define our sample of *Variable Sources* as the objects for which we detect at least one peak in the periodogram between 5 and 24 $d^{-1}$ that has a FAP less than 1%. Most other variable sources within our color cuts (slowly pulsating B-stars, RR-Lyrae variables, Cepheid variables) pulsate at frequencies below 5 $d^{-1}$ (Ridder et al. 2022), so variables which vary more rapidly than 5 $d^{-1}$ are likely $\delta$ Scuti variables.

### 3.3. *Identification of False Positives*

#### 3.3.1. *Eclipsing & Elipsoidal Binaries*

We expect the largest fraction of false positives will come from eclipsing binaries (EBs) and (to a lesser degree) ellipsoidal/contact binaries. While most EBs are

periodic at frequencies far lower than 5 $d^{-1}$, the highly non-sinusoidal shape of eclipses causes peaks in the periodogram at many integer multiples of the orbital frequency (referred to as harmonic peaks). These harmonic peaks may stretch into the frequency range we consider, meaning that harmonics can cause false-positives (Balona & Dziembowski 2011; Murphy et al. 2019; Read et al. 2024). The same argument can be made for ellipsoidal variables/contact binaries, however EBs exhibit significantly larger deviations from sinusoidal signals, so in this section we will focus on detecting EBs in particular.

To filter out these binaries we first exploit the shape of an eclipsing binary's light-curve. Figure 2 shows the first 5 days of the sector 14 QLP light-curve and resulting periodogram of the known EB TYC 2697-130-1 (TIC 14842303; Kirk et al. 2016). TYC 2697-130-1 has an orbital period of roughly 1 day, and dips by $\sim 10\%$ during each eclipse. The amplitude spectrum shows that the fundamental frequency corresponds to the half period of the orbit, since the primary and secondary eclipses are similar in size. For comparison, the bottom panels of Figure 2 show the light-curve (left) and amplitude spectrum (right) of the sector 16 photometry of $\gamma$ Boo, confirmed as a $\delta$ Scuti star by Barac et al. (2022). The periodogram is dominated by a single, strong peak at $\sim 13.6\ d^{-1}$ or $\sim 1.77$ hours. Rather than the characteristic shape of an eclipse, the variations in a $\delta$ Scuti star follow a purely, sinusoidal pattern, and therefore do not exhibit the harmonic peaks found in EBs.

By comparing these two targets we see that, while pulsations cause deviations both above and below the mean flux, eclipses will skew the average flux such that the flux of most measurements will sit above the average, unlike pulsations from a $\delta$ Scuti star. This means that a light-curve with sinusoidal behavior will have roughly half of its flux measurements below the mean, while the flux of an eclipsing binary will be above the mean more often. Thus, we define a metric, $E$, which is the fraction of points in a light-curve below the mean. This metric is similar to skewness, a statistical measurement of the lopsidedness of a distribution (see also Barbara et al. 2022).

To calibrate a threshold value for $E$ we compared two smaller samples: a sample of known eclipsing binaries (Kirk et al. 2016) and the sample of $\delta$ Scuti variables from Murphy et al. (2019). Figure 3 shows the distribution of $E$ for the *TESS* light-curves of stars in each sample. These light-curves are prepared as described in §2.2. As expected, the sample of $\delta$ Scuti stars are clustered tightly about $E = 0.5$ corresponding to 50% of flux measurements below (and above) each light curve's mean flux. The sample of eclipsing binaries extends from $E = 0.5$ to near 0. Those EBs closer to $E = 0.5$ are likely closer binaries which have more sinusoidal light-curves than more detatched binaries which will tend to have lower values of $E$. Only 0.8% of stars from the sample of $\delta$ Scuti stars fall below $E = 0.4$ while nearly 60% of the eclipsing binaries have $E < 0.4$. Applying this threshold to the *Processed Sample* yields 22,329 *Eclipsing Binaries*.

#### 3.3.2. *Distinguishing $\delta$ Scuti Stars from Other Pulsators*

$\gamma$ Doradus variables reside redwards of the instability strip, on or near to the main-sequence. They are characterized by their low frequency (i.e. $\leq 5d^{-1}$) gravity-mode ($g$-mode) pulsations (Grigahcène et al. 2010). $\gamma$ Dor and $\delta$ Scuti variables can be found in overlapping regions of the HRD. Some stars show both the $g$-modes of a $\gamma$ Dor variable and the $p$-mode oscillations of a $\delta$ Scuti variable, known as hybrid pulsators (i.e. Handler et al. 2002; Handler 2009b; Grigahcène et al. 2010; Hareter et al. 2010; Balona 2018; Antoci et al. 2019; Balona & Ozuyar 2020; Skarka, M. et al. 2022).

To help distinguish between $\delta$ Scuti and $\gamma$ Dor pulsators, we use the period-luminosity relation (PLR) of $\delta$ Scuti stars (McNamara et al. 2000, 2007; Majaess et al. 2011a; Ziaali et al. 2019; Jayasinghe et al. 2020; Poro et al. 2021, 2024; Barac et al. 2022; Read et al. 2024). Here, the period is the inverse of the frequency of the largest peak in the amplitude-spectrum ($P = \nu_0^{-1}$). We observe in Figure 4 that the majority of *Dust Corrected Variable Sources* lie along a diagonal line from roughly $\log P = -1.4$ and $M_G = 2.5$ to $\log P = -0.7$ and $M_G = 1$. However, there are also a significant number of stars at $\log P > -0.9$ and $M_G > 2$. These objects are low-luminosity and pulsate near the $5d^{-1}$ limit of our sample, which is characteristic of gravity-mode oscillations (Handler & Shobbrook 2002).

To measure the fundamental pulsation ridge we assume a relation of the form $G = m\ \log P + b$. We then fit a line to the ridge manually as an initial guess. Then, only using stars within a vertical distance of 0.45 magnitudes from that guess, we use `SciPy`'s `curve_fit` routine to perform a least-squares fit. The white line in Figure 4 marks the resulting fundamental ridge of the PLR:

$$M_G = (-2.734 \pm 0.013) \log P - (1.133 \pm 0.015) \quad (1)$$

However, there are clearly more stars above this ridge than below, particularly in the region $\log P < -1.2$, near to the Nyquist frequency. Many $\delta$ Scuti stars pulsate in the first or higher overtone rather than the fundamental mode. This manifests as a second ridge above the fundamental ridge (an example can be found in Barac et al.

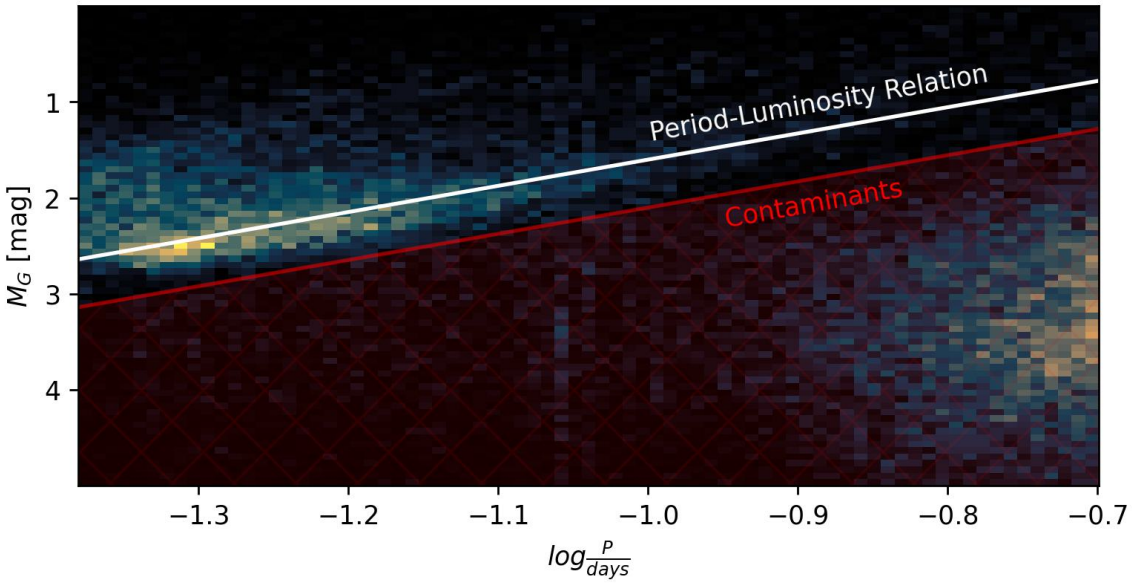


**Figure 4.** A 2-dimensional histogram showing the density of *Dust Corrected Variable Sources* as a function of their pulsation periods and absolute $G$-band magnitudes. The line $M_G = -2.734 \log P - 1.133$, marks the center of the PLR and is plotted as a solid white line. The red hatched region marks where we assume objects are *Non-δ Scuti Pulsator*s. The lower-right region has a significant over-density of presumed $\gamma$ Dor/hybrid pulsators.

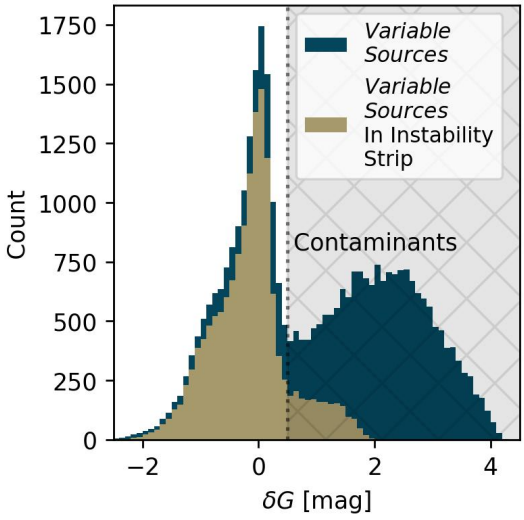


**Figure 5.** Distributions of differences between objects' observed absolute $G$-band magnitude and the magnitude implied by its pulsation period (i.e. the vertical distance from an object to the white line in Figure 4) for all *Dust Corrected Variable Sources* in blue and for just *Dust Corrected Variable Sources* within the instability strip in gold. The hatched region marks where we assume objects are *Non-δ Scuti Pulsator*s. Because $\delta G$ is in magnitudes, stars on the left-hand side of this plot, with $\delta G < 0$, lie above the PLR marked in Figure 4.

2022). By looking at the distribution of $\delta G$—the vertical distance from the PLR —as Figure 5, we identify that the peak at $\delta G = 0$ *mag* corresponds to the fundamental ridge while the overtone ridge manifests as an over density near $\delta G = -1$ *mag*, and the likely *Non-δ Scuti Pulsators* manifest as a wide distribution of objects in the hatched region of Figure 5 ($\delta G > 0.5$ *mag*).

If we assume that only stars with $\delta G < 0.5$ *mag* are *δ Scutis*, then only 15,920 out of 34,061 stars, or ∼47% of our *Dust Corrected Variable Sources* are true $\delta$ Scuti pulsators. However, this sample includes stars outside of the instability strip, where $\delta$ Scuti type pulsations are not expected. When considering only *Variable Sources* inside the instability strip (to be defined in §4]), 12,780 out of 14,707, or over 86% are *δ Scutis*, as shown in Figure 5. Meanwhile the fraction of *Non-δ Scuti Pulsators* are drastically reduced, showing that the majority of *Non-δ Scuti Pulsators* are outside of the classical instability strip.

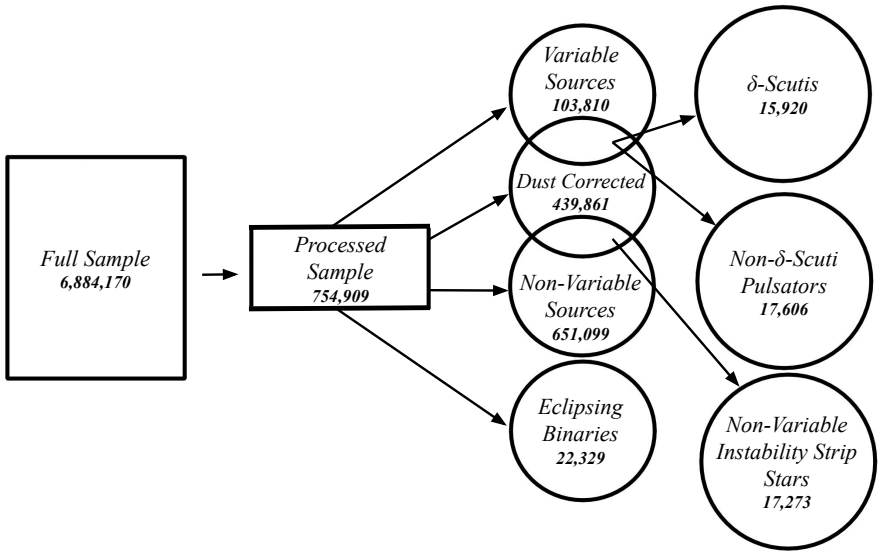


**Figure 6.** A flowchart showing the relationship between the samples named and described in §3.4

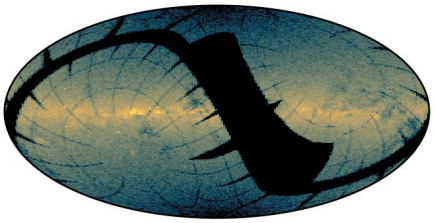

**Figure 7.** A heat-map showing the density of *Variable Sources* as a function of galactic coordinates. We detect *Variable Sources* across all *TESS* sectors, with the highest density along the Galactic plane.

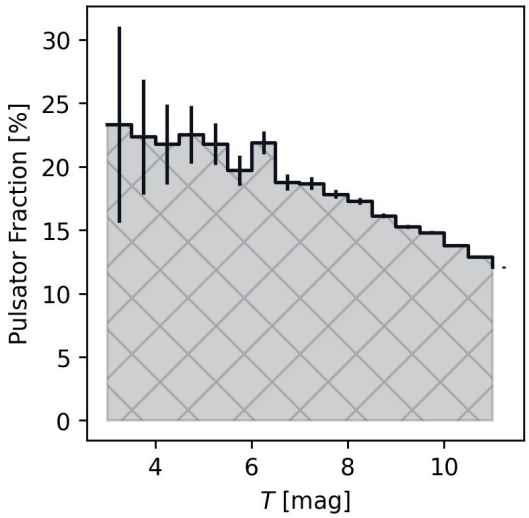


**Figure 8.** A plot showing the mean pulsator fraction across all colors as a function of apparent $T$-magnitude. Vertical lines indicate uncertainties calculated using binomial statistics, $\sigma = \sqrt{\frac{p(100-p)}{N}}$, where $p$ is the percentage of sources from the *Processed Sample* in each bin which are also *Variable Sources* and $N$ is the total number of sources from the *Processed Sample* in each bin.

### 3.4. *Summary of Stars Analyzed*

A schematic of our sample selection is shown in Figure 6. We summarize our selections as follows:

**Table 1.** Catalog of stars analyzed in this work

| *TESS* ID | Variable[a] | EB[b] | $\delta$ Scuti[c] | $\nu_0$[d] | $A_0$[e] | $N_{harmonics}$[f] | $E(G_{BP}-G_{RP})$[g] | $A_G$[h] |
|---|---|---|---|---|---|---|---|---|
| | | | | $[d^{-1}]$ | $[ppm]$ | | $[mag]$ | $[mag]$ |
| 37543035 | 1 | 0 | 0 | 6.192 | 49.51 | — | 0.009 | 0.023 |
| 37547247 | 1 | 0 | — | 19.51 | 481.8 | 0 | — | — |
| 37548587 | 1 | 0 | — | 8.786 | 3245 | 0 | — | — |
| 37571091 | 1 | 0 | 1 | 14.10 | 370.3 | 0 | 0.055 | 0.140 |
| 37576409 | 1 | 0 | — | 22.63 | 2694 | 0 | — | — |
| 37584550 | 1 | 0 | — | 6.062 | 5247 | 0 | — | — |
| 37584866 | 1 | 0 | — | 23.08 | 2046 | — | — | — |
| 37589272 | 1 | 0 | — | 5.070 | 8989 | 1 | 0.146 | 0.373 |
| 37591208 | 1 | 0 | — | 20.12 | 131.4 | — | 0.108 | 0.275 |
| 37591741 | 1 | 0 | — | 8.046 | 3265 | 0 | — | — |
| 37596454 | 1 | 0 | — | 6.838 | 87.79 | 0 | — | — |
| 37597250 | 1 | 0 | — | 16.02 | 136.1 | — | — | — |
| 37597678 | 1 | 0 | — | 5.359 | 1629 | — | — | — |
| 37599091 | 1 | 0 | 0 | 5.042 | 52.92 | — | 0.008 | 0.020 |
| 37600174 | 1 | 0 | 0 | 7.337 | 363.7 | — | 0.016 | 0.041 |
| 37601240 | 1 | 1 | 0 | 5.467 | 36920 | — | 0.015 | 0.037 |
| 37602638 | 1 | 0 | — | 21.58 | 727.4 | 0 | — | — |
| 37603872 | 1 | 0 | — | 8.127 | 4115 | 0 | — | — |
| 37605590 | 1 | 0 | — | 8.127 | 4973 | 0 | — | — |
| 37644834 | 1 | 0 | — | 6.212 | 12950 | — | 0.015 | 0.039 |

[a] denotes whether the object has at least one statistically significant peak in its periodogram between 5 and 24 $d^{-1}$ (§3.2).

[b] denotes whether the object is classified as an *Eclipsing Binary* with the $E$-metric described in §3.3.

[c] a classification of variable sources as true $\delta$ *Scutis* (1) or *Non-*$\delta$ *Scuti Pulsator*s (0) based on vertical distance from period-luminosity relation as described in §3.3.2.

[d] the frequency of the highest amplitude peak between 5 $d^{-1}$ and 24 $d^{-1}$.

[e] the amplitude corresponding to $\nu_0$, or the height of the peak associated with $\nu_0$.

[f] the number of harmonic peaks detected corresponding to integer-multiples of $\nu_0$

[g] reddening in *Gaia* color from interstellar dust.

[h] extinction in $G$-band due to interstellar dust.

- *Full Sample*[1]—§2.1—6,884,170—All stars from the *TESS* Input Catalog with $T < 13.5$ and $-0.2 < G_{BP} - G_{RP} < 1$.

- *Processed Sample*—§2.1—754,909—All stars from the *Full Sample* with $T < 11.25$ and for which at least one *TESS* sector of data between sectors 1 and 26 is available.

- *Variable Sources*—§3.2—103,810—All stars from the *Processed Sample* which have at least one statistically significant peak in its Lomb-Scargle periodogram between 5 and 24 cycles per day.

- *Non-variable Sources*—§3.2—651,099—All stars from the *Processed Sample* which did not have

[1] In the interest of clarity, when we are talking about one of the following samples of stars we will capitalize and italicize it in this text. For example, while we may refer to the broader population of $\delta$ Scuti variable stars, $\delta$ *Scutis* refer to the specific group of stars defined in this paper as $\delta$ Scuti variables.

any statistically significant peaks in its Lomb-Scargle periodogram between 5 and 24 cycles per day.

- *Dust Corrected*—§2.3—439,861—All stars from the *Processed Sample* for which we could correct for the effects of interstellar dust using the Leike et al. (2020) dust-map.
- *Eclipsing Binaries*—§3.3—22,329—All stars from the *Processed Sample* which have $E < 0.4$.
- *$\delta$ Scutis*—§3.3.2—15,920—All *Variable Sources* which are *Dust Corrected* and which do not lie below the period-luminosity relation.
- *Non-$\delta$ Scuti Pulsators*—§3.3.2—17,606—All *Variable Sources* which are *Dust Corrected* and which lie below the period-luminosity relation.
- *Non-variable Instability Strip Stars*—§4—17,273—All *Non-variable Sources* which reside within the instability strip.

Table 1 lists the quantities derived in this work. For each TIC ID analyzed we have additionally compiled information from 2 sources: the *TESS* Input Catalog (TIC) and the *Gaia* DR3 source catalog (Smith et al. 2012).

In Figure 7 we show the distribution of *Variable Sources* across the sky as a function of galactic coordinates. This shows that variability is identified over the entire sky, with most *Variable Sources* being centered on the Galactic plane. Figure 8 shows that our variability fraction declines as $T$-magnitude increases. This demonstrates that the completeness of our method is limited by the brightness of the sample.

## 4. AN EMPIRICAL INSTABILITY STRIP

Figure 9 shows pulsator fraction (the percentage of stars in each bin which are $\delta$ *Scuti* pulsators) as a function of location on the CMD. As in Murphy et al. (2019) we detect the instability strip as a pronounced ridge in the pulsator fraction plot. The pulsator fraction rises to nearly 70% at its two highest points near to $G_{BP} - G_{RP} \simeq 0.3$, $M_G = 2.5$ and $0 < M_G < 1.5$. At the red edge the pulsator fraction falls to about 0-5% whereas on the blue side pulsator fraction drops to roughly 5-15% (as measured from the bottom panel of Figure 9). Although direct comparison is not possible because Murphy et al. (2019) used effective temperatures and luminosities rather than color and magnitude, the similarity in peak pulsator fraction suggests that Kepler's selection function did not bias the population statistics derived from $\delta$ Scuti stars within the Kepler field. Further, despite the difficulties in converting to physical measurements, Figure 10 shows that for a subset of $\delta$ *Scutis* the instability strip reported in Murphy et al. (2019) fits our sample well.

Following Murphy et al. (2019), we create boundaries to this instability strip by delineating the region where pulsator fraction rises to ∼20%. We do this by drawing 20% contour lines over Figure 9, and extracting the vertices of that contour line on the blue and red edge. However, because the blue edge is not as pronounced as the red edge in color and magnitude, the blue edge of the contour is much more jagged and leads to a poor fit. To fix this we adopt the same approach as Murphy et al. (2019) and apply a Gaussian filter with a Gaussian kernel of $\sigma = 10$ to smooth the blue edge contour using Scipy's `gaussian_filter_1d`. Then, using Scipy's `curve_fit` routine we fit a straight line to the red and blue edges. Resulting in the following blue edge

$$M_G = (27.43 \pm 0.48) G_{BP} - G_{RP} - (3.0482 \pm 0.0094), \quad (2)$$

and red edge

$$M_G = (5.082 \pm 0.012) - (6.054 \pm 0.063) G_{BP} - G_{RP}. \quad (3)$$

In Figure 9, we over-plot lines representing the blue and red edges of the instability strip, chosen to align with the 20% contours, where inside this empirical instability strip the pulsator fraction is at least ∼ 20%.

## 5. A CORRELATION BETWEEN PULSATOR FRACTION AND ROTATION

Our large and homogeneous catalog allows us to investigate the occurrence of $\delta$ Scuti pulsation as a function of other physical parameters such as stellar rotation. Figure 11 shows a striking correlation of pulsator fraction with `vbroad`, this parameter is a measure of spectral line broadening from *Gaia*'s RVS spectrograph (Sartoretti et al. 2022; Frémat, Y. et al. 2023). `vbroad` is a measurement of all factors which might contribute to spectral line broadening (including $v \sin i$, mirco-turbulence, and macro-turbulence). Frémat, Y. et al. (2023) shows that for most ranges of temperature and magnitude, `vbroad` is nearly equivalent to independently measured values of $v \sin i$ up to approximately 100-200 $km\ s^{-1}$, depending on the temperature and brightness of the star. We have additionally attempted the same analysis with other sources, such as *Gaia*'s $\texttt{vsini}_{esphs}$ parameter which attempts to disentangle $v \sin i$ from other spectral line broadening phenomena (Shridharan, B. et al. 2022), as well as $v \sin i$ measurements from the Apache Point Observatory Galactic Evolution Experiment (APOGEE;

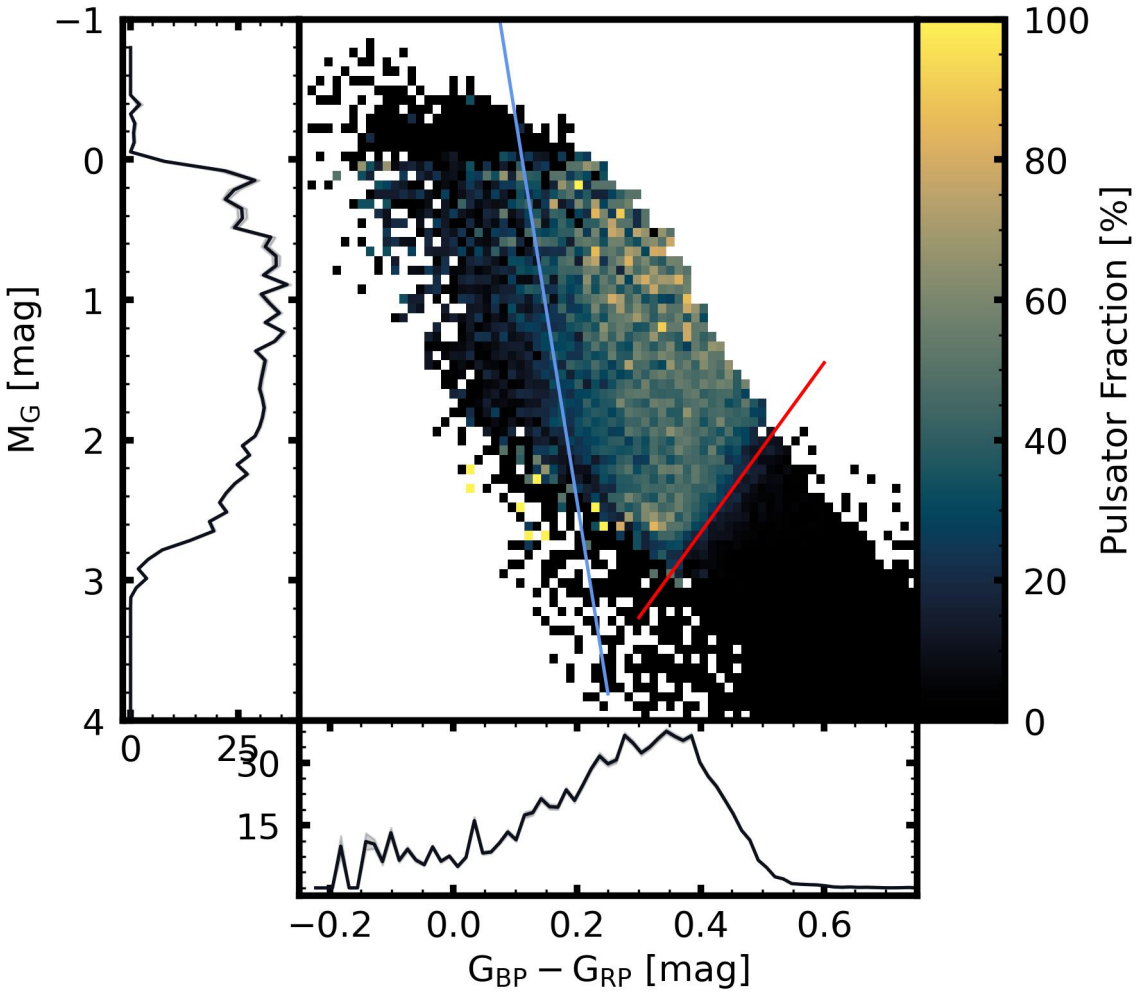


**Figure 9.** A color-magnitude diagram in which each bin is colored to represent the percentage of stars in that bin which we classify as *Variable Sources*. The bottom and left panels shows the mean pulsator fraction as a function of color and magnitude respectively. We additionally over plot lines representing the blue (Eq. 2) and red edges (Eq. 3) of the instability strip, chosen to align with the 20% contours.

Majewski et al. 2017). Both of these parameters lead to a similar observed correlation.

Since stellar $v \sin i$ is also a function of color (see Figures 10 & 12), where hot stars generally rotate more rapidly than cool stars (Kraft 1967), one simple explanation is that Figure 11 is showing that $\delta$ *Scuti* stars are on average bluer than *Non-variable*s. However, as is shown in Figure 12, $\delta$ *Scutis* have larger `vbroad` than *Non-variable Sources*, even over small regions of the CMD. The left plot of Figure 12 represents mean `vbroad` over the CMD for $\delta$ *Scuti* stars, showing that over the majority of the instability strip stars rotate at velocities between 100 and 250 km/s. The *Non-variable Sources* are shown on the right, where we show that over the majority of the instability strip, *Non-variable Sources* rotate at velocities below 100 km/s.

One possible explanation for this effect is rotational mixing (Owocki et al. 1996; Maeder 1998; Huang 2004). Since the $\kappa$-mechanism relies on the partial ionization of helium in a specific layer of a star's atmosphere, a star requires helium in that layer for classical pulsations to occur. As stars age, if they are not steadily mixed, they become chemically stratified, as heavier elements gravitationally settle to lower layers within the star. This is in agreement with findings of low pulsation fractions among the slow-rotating, metalically-lined A-stars (Breger 1970; Pamjatnykh 1974; Kurtz 1989; Ouazzani et al. 2015). Should helium gravitationally settle below the partial ionization layer in a $\delta$ Scuti variable, the driving of those pulsations will weaken. As described by Murphy et al. (2015), non-pulsators in the instability strip may be those that are magnetically active and slowly rotating. Our catalog yields a sample of bright,

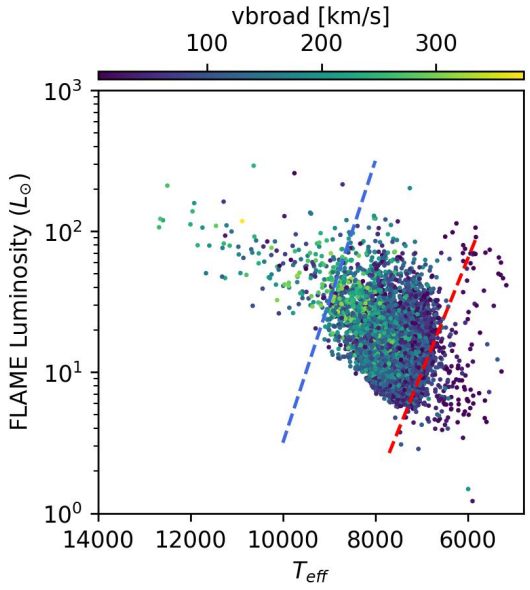


**Figure 10.** A Hertzsprung-Russell diagram of $\delta$ Scuti variables, colored by the Gaia line broadening measure `vbroad`. Luminosities are from FLAME (Fouesneau, M. et al. 2023), and $T_{eff}$ comes from two sources. For the hotter stars ($T > 9000$ $K$) we use spectroscopic *Gaia* ESPHS measurements, however ESPHS does not cover the entire instability strip, so for cooler stars we use GSPPHOT measurements (Shridharan, B. et al. 2022). Dashed lines show the instability strip reported in Murphy et al. (2019).

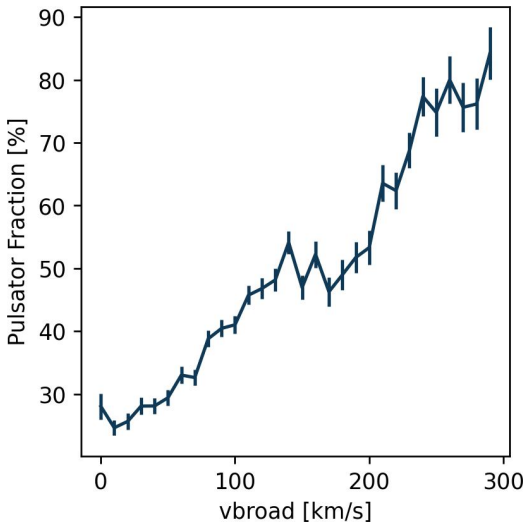


**Figure 11.** Pulsator fraction (the percentage of *Dust Corrected* stars inside of the instability strip in each bin classified as $\delta$ *Scutis*) as a function of `vbroad`. Vertical lines indicate uncertainties calculated using binomial statistics, $\sigma = \sqrt{\frac{p(100-p)}{N}}$, where $p$ is the percentage of sources from the *Processed Sample* in each bin which are also *Variable Sources* and $N$ is the total number of sources from the *Processed Sample* in each bin.

*Non-variable Instability Strip Stars*, which are ideal targets for follow-up with high resolution spectroscopy to confirm this hypothesis.

## 6. CONCLUSION

By analyzing nearly one million 30-minute cadence *TESS* QLP light-curves with $T < 11.25$ (Huang et al. 2020a,b; Kunimoto et al. 2021) we have identified variability in 103810 sources and confirmed 15,920 $\delta$ *Scuti* variables. This is an order of magnitude leap in the search for classical pulsators compared to the Kepler field and utilizes data with an extremely simple selection function. Our main conclusions are as follows:

- We measure a period-luminosity relation ($M_G = (-2.734 \pm 0.013)\log_{10} P - (1.133 \pm 0.015)$ where $P$ is the pulsation period measured in days) and identify contaminating stars which are presumably either EBs, hybrid $p/g$-mode pulsators, or $g$-mode pulsators.
- After identifying $\delta$ *Scuti* pulsators, we calculate pulsator fraction across the color-magnitude diagram (CMD) and produce boundaries for an empirical instability strip in observed *Gaia* parameters—$G_{BP} - G_{RP}$ and $M_G$ (equations 2 and 3). Consistent with previous investigations we find that, even in the center of the instability strip over 20% of sources show no pulsations. This instability strip drops off sharply on the red-side to near 0% and slopes more gently on the blue side to ∼10-20%.
- We show that *Gaia*'s `vbroad` parameter—a measure of spectral line broadening—is systematically larger for $\delta$ *Scuti* sources than for their non-pulsating cousins. This pattern holds even when controlling for location in the CMD. This correlation confirms that rotation plays a crucial role in sustaining classical pulsations. We hypothesize that more slowly rotating A-F stars become more chemically stratified, allowing helium to gravitationally settle below the partial ionization layer where the $\kappa$-mechanism drives classical pulsations.

This work naturally suggests a few lines of inquiry to follow in the future. For one, the procedures outlined in this work could be replicated for other types of pulsators. For example, $\gamma$ Doradus pulsators reside within similar regions of the CMD. $\gamma$ Doradus variables pulsate in non-radial $g$-modes and simply extending the range of frequencies analyzed would likely find a significant number of $\gamma$ Doradus variables in the region red-ward of the instability strip. Similarly, higher-cadence data, such as

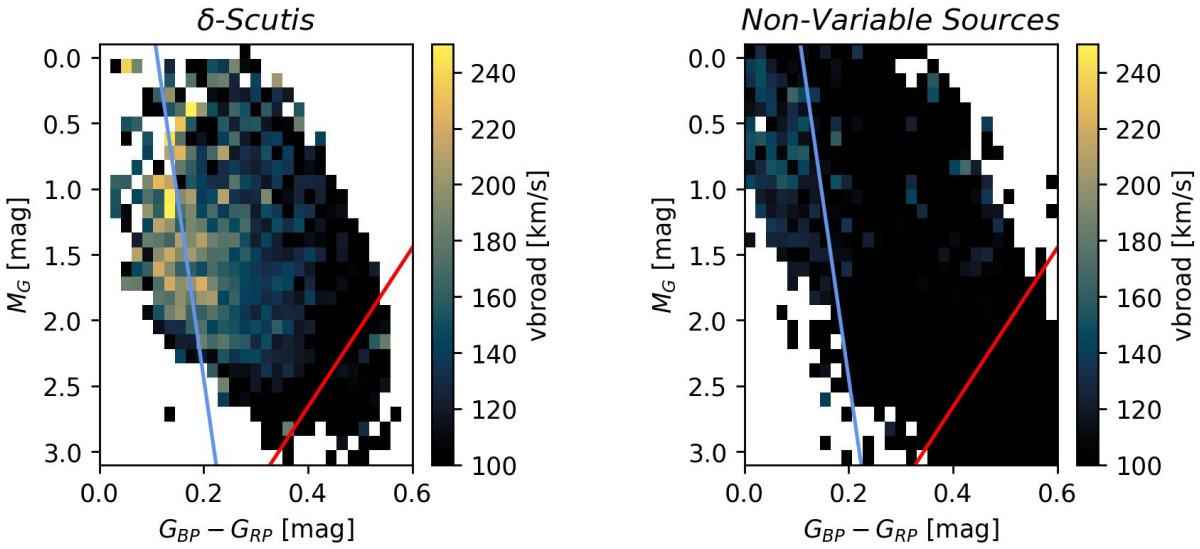


**Figure 12.** A CMD colored by the mean `vbroad` values of $\delta$ *Scuti* variables (left) and *Non-variable*s (right) in each bin. Only bins with at least 10 objects are shown. Note that any bin with a value below 100 km/s is colored black, meaning that *Non-variables*—over most of the cmd—have values of `vbroad` below 100 km/s. $\delta$ *Scuti*s, however, show `vbroad` values over 100 km/s over most of the instability strip. We additionally over-plot lines representing the blue and red edges of the instability strip.

the 600s cadence data available in later *TESS* cycles, could capture higher-frequency pulsators, such as young $\delta$ Scuti stars (Bedding et al. 2020). Finally, an analysis including pixel-level data analysis (e.g. Higgins & Bell 2022) would be helpful to disentangle different sources of variability in crowded fields.

K.G. and D.H. acknowledge support from the the National Aeronautics and Space Administration through the TESS General Investigator Program (80NSSC21K0784). M.H. acknowledges support from NASA through the NASA Hubble Fellowship grant HST-HF2-51459.001 awarded by the Space Telescope Science Institute, which is operated by the Association of Universities for Research in Astronomy, Incorporated, under NASA contract NAS5-26555. D.H. also acknowledges support from the Alfred P. Sloan Foundation and the Australian Research Council (FT200100871). D.R.H. acknowledges support from the National Science Foundation (AST-2009828). T.R.B. and S.J.M. gratefully acknowledge support from the Australian Research Council through Future Fellowship FT210100485 and Laureate Fellowship FL220100117.

Funding for the TESS mission is provided by NASA's Science Mission directorate. This paper includes data collected by the TESS mission, which are publicly available from the Mikulski Archive for Space Telescopes (MAST).

*Software:* This research made use of `NumPy` version 1.24.3 (Harris et al. 2020), `pandas` version 2.1.4 (McKinney 2010; team 2023), `AstroPy` version 5.3.4 (Robitaille et al. 2013; Price-Whelan et al. 2018), `SciPy` version 1.11.4 (Virtanen et al. 2020). All plots were made using `matplotlib` version 3.7.2 (Hunter 2007; Caswell et al. 2023), Figure 10 makes use of `matplotlib`'s `viridis` colormap, and the remaining plots use the `eclipse` colormap from `CMasher` (van der Velden 2020).

## REFERENCES

Antoci, V., Cunha, M., Bowman, D., et al. 2019, Monthly Notices of the Royal Astronomical Society, doi: 10.1093/mnras/stz2787

Balona, L. A. 2018, Monthly Notices of the Royal Astronomical Society, 479, 183, doi: 10.1093/mnras/sty1511

—. 2024, The Open Journal of Astrophysics, 7, doi: 10.21105/astro.2109.12574

Balona, L. A., & Dziembowski, W. A. 2011, Monthly Notices of the Royal Astronomical Society, 417, 591, doi: 10.1111/j.1365-2966.2011.19301.x

Balona, L. A., & Ozuyar, D. 2020, Monthly Notices of the Royal Astronomical Society, 493, 5871, doi: 10.1093/mnras/staa670

Baluev, R. V. 2008, Monthly Notices of the Royal Astronomical Society, 385, 1279, doi: 10.1111/j.1365-2966.2008.12689.x

Barac, N., Bedding, T. R., Murphy, S. J., & Hey, D. R. 2022, Monthly Notices of the Royal Astronomical Society, 516, 2080, doi: 10.1093/mnras/stac2132

Barbara, N. H., Bedding, T. R., Fulcher, B. D., Murphy, S. J., & Van Reeth, T. 2022, Monthly Notices of the Royal Astronomical Society, 514, 2793, doi: 10.1093/mnras/stac1515

Barceló Forteza, S., Roca Cortés, T., & García, R. A. 2018, A&A, 614, A46, doi: 10.1051/0004-6361/201731803

Batalha, N. M., Borucki, W. J., Koch, D. G., et al. 2010, The Astrophysical Journal Letters, 713, L109, doi: 10.1088/2041-8205/713/2/L109

Bedding, T. R., Murphy, S. J., Hey, D. R., et al. 2020, Nature, 581, 147, doi: 10.1038/s41586-020-2226-8

Bedding, T. R., Murphy, S. J., Crawford, C., et al. 2023, The Astrophysical Journal Letters, 946, L10, doi: 10.3847/2041-8213/acc17a

Bowman, D. M., & Kurtz, D. W. 2018, Monthly Notices of the Royal Astronomical Society, 476, 3169, doi: 10.1093/mnras/sty449

Breger, M. 1970, Astrophysical Journal, 162, 597, doi: 10.1086/150691

—. 1979, Publications of the Astronomical Society of the Pacific, 91, 5, doi: 10.1086/130433

Caswell, T. A., Andrade, E. S. d., Lee, A., et al. 2023, matplotlib/matplotlib: REL: v3.7.2, Zenodo, doi: 10.5281/zenodo.8118151. https://doi.org/10.5281/zenodo.8118151

Choi, J., Dotter, A., Conroy, C., et al. 2016, The Astrophysical Journal, 823, 102, doi: 10.3847/0004-637X/823/2/102

Dotter, A. 2016, The Astrophysical Journal Supplement Series, 222, 8, doi: 10.3847/0067-0049/222/1/8

Dupret, M.-A., Grigahcène, A., Garrido, R., Gabriel, M., & Scuflaire, R. 2004, A&A, 414, L17, doi: 10.1051/0004-6361:20031740

—. 2005, A&A, 435, 927, doi: 10.1051/0004-6361:20041817

Dziembowski, W. 1980, in Nonradial and Nonlinear Stellar Pulsation, ed. H. A. Hill & W. A. Dziembowski (Berlin, Heidelberg: Springer Berlin Heidelberg), 22–33

Fitzpatrick, E. L. 1999, Publications of the Astronomical Society of the Pacific, 111, 63, doi: 10.1086/316293

Fouesneau, M., Frémat, Y., Andrae, R., et al. 2023, A&A, 674, A28, doi: 10.1051/0004-6361/202243919

Frémat, Y., Royer, F., Marchal, O., et al. 2023, A&A, 674, A8, doi: 10.1051/0004-6361/202243809

Goupil, M. J., Dupret, M. A., Samadi, R., et al. 2005, Journal of Astrophysics and Astronomy, 26, 249, doi: 10.1007/BF02702333

Green, G. M. 2018, Journal of Open Source Software, 3, 695, doi: 10.21105/joss.00695

Grigahcène, A., Uytterhoeven, K., Antoci, V., et al. 2010, Astronomische Nachrichten, 331, 989, doi: https://doi.org/10.1002/asna.201011443

Guzik, J. A. 2021, Frontiers in Astronomy and Space Sciences, 8, doi: 10.3389/fspas.2021.653558

Guzik, J. A., Fontes, C. J., & Fryer, C. 2018, Atoms, 6, doi: 10.3390/atoms6020031

Guzik, J. A., Jackiewicz, J., Catanzaro, G., & Soukup, M. S. 2021, Characterizing Variability in Bright Metallic-Line A (Am) Stars Using Data from the NASA TESS Spacecraft

Handler, G. 2009a, in American Institute of Physics Conference Series, Vol. 1170, Stellar Pulsation: Challenges for Theory and Observation, ed. J. A. Guzik & P. A. Bradley, 403–409

Handler, G. 2009b, Monthly Notices of the Royal Astronomical Society, 398, 1339, doi: 10.1111/j.1365-2966.2009.15005.x

Handler, G., & Shobbrook, R. R. 2002, Monthly Notices of the Royal Astronomical Society, 333, 251, doi: 10.1046/j.1365-8711.2002.05401.x

Handler, G., Balona, L. A., Shobbrook, R. R., et al. 2002, Monthly Notices of the Royal Astronomical Society, 333, 262, doi: 10.1046/j.1365-8711.2002.05295.x

Hareter, M., Reegen, P., Miglio, A., et al. 2010, Gamma Dor and Gamma Dor - Delta Sct Hybrid Stars In The CoRoT LRa01, Tech. rep.

Harris, C. R., Millman, K. J., Walt, S. J. v. d., et al. 2020, Nature, 585, 357, doi: 10.1038/s41586-020-2649-2

Hasanzadeh, A., Safari, H., & Ghasemi, H. 2021, Monthly Notices of the Royal Astronomical Society, 505, 1476, doi: 10.1093/mnras/stab1411

Hey, D. R., Montet, B. T., Pope, B. J. S., Murphy, S. J., & Bedding, T. R. 2021, The Astronomical Journal, 162, 204, doi: 10.3847/1538-3881/ac1b9b

Higgins, M. E., & Bell, K. J. 2022, Astrophysics Source Code Library, ascl:2204.005

Huang, C. X., Vanderburg, A., Pál, A., et al. 2020a, Research Notes of the American Astronomical Society, 4, 204, doi: 10.3847/2515-5172/abca2e

—. 2020b, Research Notes of the American Astronomical Society, 4, 206, doi: 10.3847/2515-5172/abca2d

Huang, R. Q. 2004, Astronomy & Astrophysics, 425, 591, doi: 10.1051/0004-6361:20034245

Hunter, J. D. 2007, Computing in Science & Engineering, 9, 90, doi: 10.1109/MCSE.2007.55

Jayasinghe, T., Stanek, K. Z., Kochanek, C. S., et al. 2020, Monthly Notices of the Royal Astronomical Society, 493, 4186, doi: 10.1093/mnras/staa499

Kirk, B., Conroy, K., Prša, A., et al. 2016, The Astronomical Journal, 151, 68, doi: 10.3847/0004-6256/151/3/68

Kraft, R. P. 1967, The Astrophysical Journal, 150, 551, doi: 10.1086/149359

Kunimoto, M., Huang, C., Tey, E., et al. 2021, Research Notes of the American Astronomical Society, 5, 234, doi: 10.3847/2515-5172/ac2ef0

Kurtz, D. W. 1989, Monthly Notices of the Royal Astronomical Society, 238, 1077, doi: 10.1093/mnras/238.3.1077

—. 2022, Annual Review of Astronomy and Astrophysics, 60, 31, doi: 10.1146/annurev-astro-052920-094232

Leavitt, H. S. 1908, Annals of Harvard College Observatory, 60, 87

Leike, R. H., Glatzle, M., & Enßlin, T. A. 2020, Astronomy and Astrophysics, 639, A138, doi: 10.1051/0004-6361/202038169

Lomb, N. R. 1976, Astrophysics and Space Science, 39, 447, doi: 10.1007/BF00648343

Maeder, A. 1998, in Astronomical Society of the Pacific Conference Series, Vol. 131, Properties of Hot Luminous Stars, ed. I. Howarth, 85

Majaess, D. J., Turner, D. G., Lane, D. J., Henden, A., & Krajci, T. 2011a, JAVSO, 39, 122

Majaess, D. J., Turner, D. G., Lane, D. J., & Krajci, T. 2011b, JAVSO, 39, 219

Majewski, S. R., Schiavon, R. P., Frinchaboy, P. M., et al. 2017, The Astronomical Journal, 154, 94, doi: 10.3847/1538-3881/aa784d

McKinney, W. 2010, in Proceedings of the 9th Python in Science Conference, ed. S. v. d. Walt & J. Millman, 56 – 61

McNamara, D., Madsen, J., Barnes, J., & Ericksen, B. 2000, Publications of the Astronomical Society of the Pacific, 112, 202, doi: 10.1086/316512/XML

McNamara, D. H., Clementini, G., & Marconi, M. 2007, The Astronomical Journal, 133, 2752, doi: 10.1086/513717/FULLTEXT/

Molenda-Zakowicz, J., Arentoft, T., Frandsen, S., & Grundahl, F. 2009, Rotation of delta Scuti Stars in the Open Clusters NGC1817 and NGC7062, arXiv. http://arxiv.org/abs/0907.0812

Murphy, S. J., Bedding, T. R., Niemczura, E., Kurtz, D. W., & Smalley, B. 2015, Monthly Notices of the Royal Astronomical Society, 447, 3948, doi: 10.1093/mnras/stu2749

Murphy, S. J., Hey, D., Van Reeth, T., & Bedding, T. R. 2019, Monthly Notices of the Royal Astronomical Society, 485, 2380, doi: 10.1093/MNRAS/STZ590

Ouazzani, R.-M., Roxburgh, I. W., & Dupret, M.-A. 2015, Astronomy & Astrophysics, 579, A116, doi: 10.1051/0004-6361/201525734

Owocki, S. P., Cranmer, S. R., & Gayley, K. G. 1996, The Astrophysical Journal, 472, L115, doi: 10.1086/310372

Pamjatnykh, A. A. 1974, Nauchnye Informatsii, 32, 104

Paxton, B., Bildsten, L., Dotter, A., et al. 2010, The Astrophysical Journal Supplement Series, 192, 3, doi: 10.1088/0067-0049/192/1/3

Paxton, B., Cantiello, M., Arras, P., et al. 2013, The Astrophysical Journal Supplement Series, 208, 4, doi: 10.1088/0067-0049/208/1/4

Paxton, B., Marchant, P., Schwab, J., et al. 2015, The Astrophysical Journal Supplement Series, 220, 15, doi: 10.1088/0067-0049/220/1/15

Poro, A., Paki, E., Mazhari, G., et al. 2021, Publications of the Astronomical Society of the Pacific, 133, 084201, doi: 10.1088/1538-3873/ac12dc

Poro, A., Jafarzadeh, S. J., Harzandjadidi, R., et al. 2024, Period-Luminosity Relationship for $\delta$ Scuti Stars Revisited, doi: 10.48550/arXiv.2401.01091. https://ui.adsabs.harvard.edu/abs/2024arXiv240101091P

Price-Whelan, A. M., Sipőcz, B. M., Günther, H. M., et al. 2018, The Astronomical Journal, 156, 123, doi: 10.3847/1538-3881/aabc4f

Read, A. K., Bedding, T. R., Mani, P., et al. 2024, Monthly Notices of the Royal Astronomical Society, doi: 10.1093/mnras/stae165

Ricker, G. R., Winn, J. N., Vanderspek, R., et al. 2015, Journal of Astronomical Telescopes, Instruments, and Systems, 1, 14003, doi: 10.1117/1.JATIS.1.1.014003

Ridder, J. D., Ripepi, V., & Aerts, C. 2022, Astronomy & Astrophysics, doi: 10.1051/0004-6361/202243767

Robitaille, T. P., Tollerud, E. J., Greenfield, P., et al. 2013, Astronomy & Astrophysics, 558, A33, doi: 10.1051/0004-6361/201322068

Sartoretti, P., Blomme, R., David, M., & Seabroke, G. M. 2022, Gaia Data Release 3 Documentation release 1.1. https://gea.esac.esa.int/archive/documentation/GDR3/Data_processing/chap_cu6spe/

Scargle, J. D. 1982, The Astrophysical Journal, 263, 835, doi: 10.1086/160554

Shridharan, B., Mathew, B., Bhattacharyya, S., et al. 2022, A&A, 668, A156, doi: 10.1051/0004-6361/202244353

Skarka, M., Žák, J., Fedurco, M., et al. 2022, A&A, 666, A142, doi: 10.1051/0004-6361/202244037

Smith, N., Aghakhanloo, M., Murphy, J. W., et al. 2012, Mon. Not. R. Astron. Soc, 000

Solano, E., & Fernley, J. 1997, Astronomy and Astrophysics Supplement Series, 122, 131, doi: 10.1051/aas:1997329

team, T. p. d. 2023, pandas-dev/pandas: Pandas, Zenodo, doi: 10.5281/zenodo.10304236. https://doi.org/10.5281/zenodo.10304236

van der Velden, E. 2020, The Journal of Open Source Software, 5, 2004, doi: 10.21105/joss.02004

VanderPlas, J. T. 2018, The Astrophysical Journal Supplement Series, 236, 16, doi: 10.3847/1538-4365/aab766

Virtanen, P., Gommers, R., Oliphant, T. E., et al. 2020, Nature Methods, 17, 261, doi: 10.1038/s41592-019-0686-2

Wolniewicz, L. M., Berger, T. A., & Huber, D. 2021, The Astronomical Journal, 161, 231, doi: 10.3847/1538-3881/abee1d

Xue, W., Niu, J.-S., Xue, H.-F., & Yin, S. 2023, Research in Astronomy and Astrophysics, 23, 075002, doi: 10.1088/1674-4527/accdbc

Ziaali, E., Bedding, T. R., Murphy, S. J., Van Reeth, T., & Hey, D. R. 2019, Monthly Notices of the Royal Astronomical Society, 486, 4348, doi: 10.1093/mnras/stz1110